The 4th European sCO2 Conference for Energy Systems
March 23-24, 2021, Online Conference

2021-sCO2.eu-110

MICROSTRUCTURAL EVALUATION OF PRESELECTED STEELS FOR TURBINE AFTER SUPERCRITICAL CO2 EXPOSURE

Lucia Rozumová*
Centrum vyzkumu Rez s.r.o.
Hlavní 130, Husinec-Rez, Czech Republic
Email: lucia.rozumova@cvrez.cz

Tomáš Melichar*
Centrum vyzkumu Rez s.r.o.
Hlavní 130, Husinec-Rez, Czech Republic
Email: tomas.melichar@cvrez.cz

Ladislav Velebil
Centrum vyzkumu Rez s.r.o.
Hlavní 130, Husinec-Rez, Czech Republic

ABSTRACT

The energy conversion cycles with supercritical carbon dioxide (sCO2) are being considered as an innovative technology with potential for replacement of conventional steam cycles within various applications such as nuclear, fossil or renewable energy resources. Due to extreme operational conditions including temperatures above 550°C and pressures up to 25 MPa, proper selection of materials is essential for a suitable design of the thermal circuit. Several materials that were identified as potentially suitable for the main components of the sCO2 circuits were exposed in the sCO2 relevant conditions in the sCO2 experimental loop at Research Centre Rez (CVR). The experimental conditions were represented by the sCO2 temperature of 550°C, pressure of 25 MPa, flow conditions and 1000 hours of exposure. Moreover, an additional test section where the sCO2 flow velocity up to 100 m/s was achieved was designed and utilized to simulate turbine relevant conditions.

Suitability of the materials preselected for the sCO2 turbomachinery will be evaluated and discussed in this paper. For the experiments, four types of materials (FB2, 17-4-PH, 625M, IN718) were selected. After the exposure, the corrosion behaviour and oxidation of the materials was investigated including surface analyses and cross sections examination. The paper presents the experimental parameters including the high velocity test section design. The materials degradation will be evaluated as well as the effect of the high velocity flow.

INTRODUCTION

The worldwide interest in the supercritical dioxide power cycle has increased steadily in the last decade. The use of CO2 as a working fluid in a power cycle has been proposed by several researchers as a novel and promising cycle. The possibility of high efficiency is very encouraging. Benefits of smaller turbomachinery and other parts compared to the parts of conventional steam cycles are obvious [1].

As a kind of efficient energy conversion system, the supercritical carbon dioxide (sCO2) power generation system attracts increasing attention due to the advancement of its compact structure and the potential to improve the conversion efficiency. The use of carbon dioxide (CO2) as a working fluid might produce higher efficiencies comparing to other gases due to unique thermodynamic properties (especially density changes near to the critical point) [2]. Supercritical carbon dioxide (sCO2) is currently being considered as a working fluid fora Brayton cycle in next generation power systems for uses across nuclear, solar, and fossil power sources [3, 4, 5].

The safety is a critical for the design and operation of the sCO2 cycle and material selection is one of the most important elements for long-term safe and stable operation of this power system. However, current research on the corrosion behaviour in high-temperature sCO2 is still not fully understood [6, 7, 8]. The main topics for research and publication are turbomachinery, heat exchangers and new cycle proposals. The great interest expressed by the scientific community aims to theoretical analysis of the thermodynamic principles of the sCO2 power cycle [9, 10]. Last but not least, the extensive research on the corrosion behaviour of commercial steels and alloys in high-temperature sCO2 under different operating conditions is desirable and inevitable.

The corrosion study of 9Cr, 12Cr, and 18Cr steels in high-temperature sCO2 for long-term compatibility tests for reactors with a design life of 60 years studied Furukawa et al. [11]. Holcomb et al. investigated the corrosion behaviour of austenitic heat-resistant steels and Ni-base alloys in sCO2 environments [12]. The carburization behaviour of Fe–20Cr (wt.%) alloy in Ar-20CO2 at 650 °C studied the research group of Young et al [13]. Rouillard et al. investigated the oxidation

* corresponding author(s)

DOI: 10.17185/duepublico/73951

and carburization behaviour of 9Cr steel in high-temperature CO2 [14]. Corrosion and carburization behaviour of heat-resistant steels in a high-temperature supercritical carbon dioxide environment was evaluated in Goi´s work [15]. Tan in his work evaluated Corrosion of austenitic and ferritic-martensitic steels exposed to supercritical carbon dioxide [16]. The mechanisms of carburization and of oxide failure are described Grabke in his work, and the measures and methods for control and prevention of carburization are evaluated, too [17, 18]. Carburisation of ferritic model Fe–Cr alloys by low carbon activity gases was examined in paper by Gheno [19].

It is very important to evaluate the corrosion performance and resistance including the oxidation and carburization of the key component materials in a high-temperature sCO2 environment. Therefore, this paper aims to investigate the evaluation of pre-selected construction materials, corrosion resistance of four kinds of steels and alloys used in advanced thermal power generation systems in a high-temperature sCO2 environment.

EXPERIMENTAL SYSTEM AND MATERIALS

To be able to carry out more in deep research in sCO2 technologies the highly modular sCO2 loop has been built in CVR as part of The Sustainable Energy Project (SUStainable ENergy, SUSEN). SUSEN targeted to strengthen the research, development and innovative capabilities of the Czech Republic, which would enable raise of competitiveness and create highly qualified jobs to make the regions of the Czech Republic become important points of concentration of such activities in Europe.

Wide variety of research can be done at given loop. Such as heat transfer experiments, erosion, corrosion testing etc. The main operating parameters are:

- Max. operating temperature: 550°C
- Max pressure at high pressure site: 30 MPa
- Max. pressure at low pressure site: 15 MPa
- Max. flow rate: 0.35 kg.s^{-1}
- Total heating power: 110 kW

The main configuration is shown at simplified diagram Fig. 1.

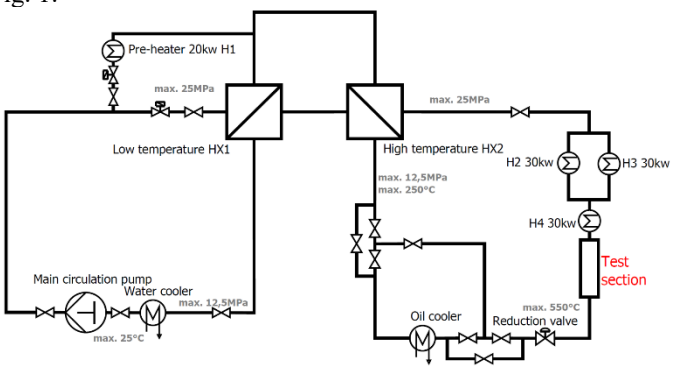

Figure 1: Simplified diagram of sCO2 loop

The material samples for experiment had to be placed in predesigned test section, where the parameters of medium were regulated to the demanded values. The samples where hold on place by tailored sample holder, which can be used again and again.

Design of test section

By nature, the sample holder has to be placed inside the test section (Fig. 2), which has following dimensions: 2 m in length and 58mm in inside diameter. The section is made from alloy Inconel 625. Both ends are flanged for easy assembly and disassembly. Holder itself consist from two main body parts. Corrosion (Fig. 2) and erosion part (Fig. 2), where the flow is accelerated by three narrow channels to 100 m.s^{-1} at given parameters 20 MPa, 500 °C and mass flow 0.1 kg.m^{-1} and possibly even to higher stats.

Corrosion and erosion part

Main element of the corrosion part is its base, which has to insure anchoring the samples at predefined position and allows to use variety of samples of different dimensions. The dimensions are 10x2, 10x5, 20x2 and 40x4. For dimension 50x3 there is a base alone. Their length is not determined, and their thickness can be smaller. The given number is just its maximum value. Bases where cut out from sheet of metal and melted together. Through the centre goes shaft to detain pieces at their predesigned positions. On each part was used coating TiAlSiN (trading mark, MARVIN Si) from Czech company SHM s.r.o. This coating was intentionally selected so the nonconductive connection could be maintained and also disassembly was much easier after test run.

The erosion part was designed and optimized to reach high velocities in the narrow channels in order to simulate the flow conditions on the turbine blades. Results given by CFD calculations show that the current design reach pressure drop of 1.1 MPa and average velocity through the narrow channel is 105.6 m.s^{-1}.

Many drafts were considered and processed till high level of design. As it's very common, several contradictory requirements had to be met. Main problem was linked with acceleration of the flow. From 0.1 kg.s^{-1} at 550 °C and 20 MPa on diameter 58mm it had to be forced into very narrow channel to achieve at least 100m.s^{-1}. Such a doing was non-negotiable and caused that final product had to be very demanding on manufactured and assemble precision. First half of the timespan of the design was therefore spend on finding solution, which could be manufactured, hopefully with ease, wouldn't be expensive and would perfectly meet the demands of the experiment on conditions, which has to be on material samples. To meet them, the section has to be perfectly sealed. Cause if it wouldn't, the flow which would go through leakage would cause velocity drop and requirement on velocity of the flow wouldn't be met. For these temperatures rubber, teflon or similar materials are out of the table, they wouldn't endure them. Mainly two possible options were evaluated. Some kind of graphite sealing or so called "metal to metal" sealing.

Graphite sealing with its less demands on surface finish was chosen over "metal to metal." How to divide the part to subparts and still be able to seal the thing, was the catch. Different overall symmetries, shapes of channels, division into components etc. was considered. As the final solution the design with 1/3 symmetry was chosen and it consist of main body part, graphite sealings, wedges and parts which acts as pressers to the sealings and holds samples at their place (Fig. 2) with only the need to seal the samples, so the flow wouldn't go behind them and to seal the sample holder outer diameter with inner diameter of the test section.

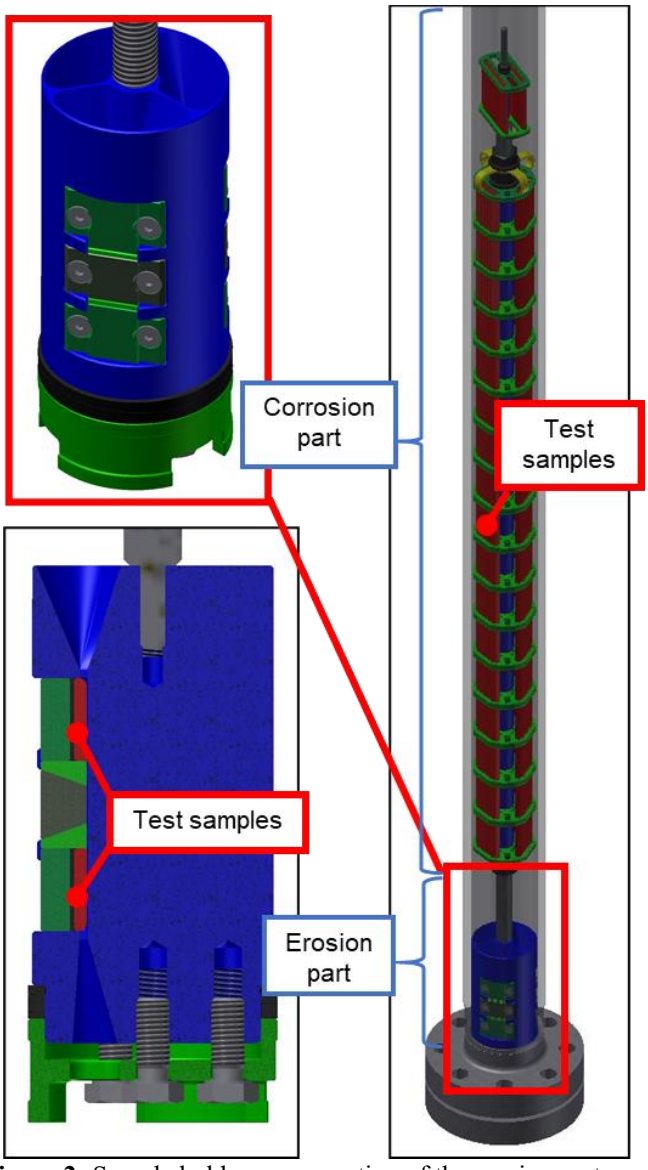

Figure 2: Sample holder, cross-section of the erosion part

This is done with graphite rope with dimensions 4x4mm. For the graphite to work properly as a sealing, it has to be more then mildly pressed. This is done by pressers at samples and for outer-inner diameter it's done by inner flange. Erosion part was very demanding to be manufactured and on assemble precision. For main body part the method of 3D printing was consider. Unfortunately, the demand on surface roughness in the channel would not be possible to meet. Therefore, conventional machining had to do this job. Whole erosion part can take up to 6 pieces of samples of dimensions 20x10x3.

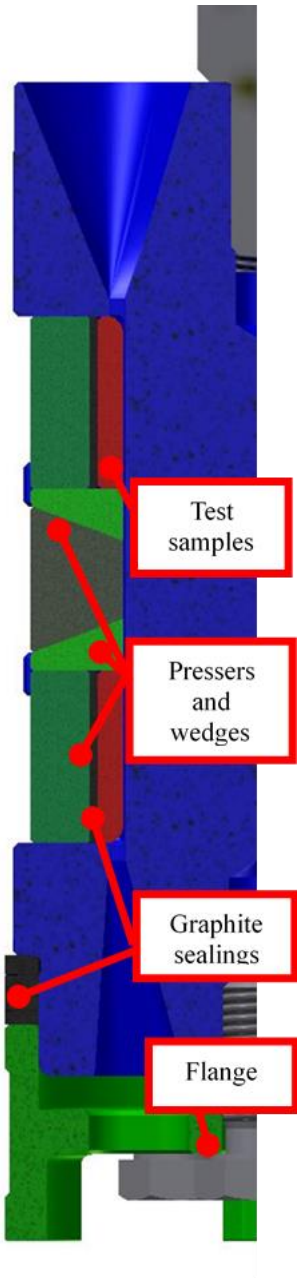

Figure 3: Cross-section of the erosion part

Assembling

At first all samples were imprinted with a mark, then cleaned with ethanol and acetylene by ultrasonic cleaner, weighed and those figures noted. Then all parts of sample holder where cleaned by same procedure. Assembling was carried out in clean

environment. Assembled sample holder is shown at Fig. 4. The test section is stationed vertically, therefore the sample holder has to be somehow anchored in the section. This is done when test section lays in horizontal position when dissemble. Sample holder is put inside at given place, where when it is in vertical position it can rest at inner edge of lower flange, which goes few millimetres inside. Before moving the section into its place in the loop, the graphite sealing at outside diameter of erosion part is pressed by inner section flange. This pressure can produce force big enough to counter gravity while sample holder is being transferred to its place.

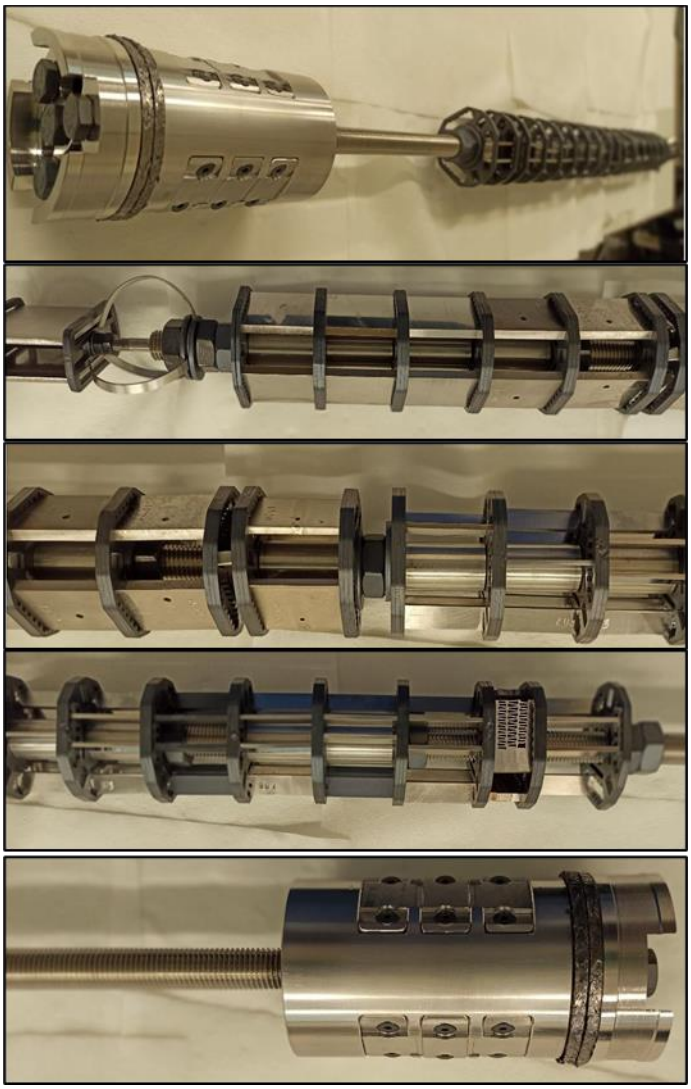

Figure 4: Assembled sample holder

Materials and test conditions

The experimental materials included four kinds of high-grade heat-resistant alloys, 9-12% Cr steel (FB2), martensitic precipitation-hardening stainless steel (17-4-PH), nickel-based superalloy (625M), corrosion-resistant nickel alloy (Inconel 718), which have been widely employed in various energy conversion, power plants, and nuclear industries because of its exceptional properties of high-temperature strength and creep resistance. The chemical compositions of the studied materials are listed in Table 1.

Martensitic stainless steel, FB2 is the creep resistant steel, which was manufactured and developed for turbine rotor forging. It is 9-12% Cr boron-containing steel, primarily for steam temperatures ≥ 620°C. 17-4-PH is a chromium-nickel-copper precipitation-hardening martensitic stainless steel with an addition of niobium. 17-4-PH combines high strength and hardness with good corrosion resistance. Alloy 625M is a nickel-based superalloy that possesses high strength properties and resistance to elevated temperatures. It also demonstrates remarkable protection against corrosion and oxidation. It has the ability to withstand high stress and a wide range of temperatures, as well as being able to resist corrosion while being exposed to highly acidic environments. Alloy In718 is a high-strength, corrosion-resistant nickel chromium material. The age-hard enable alloy has resistance to post weld cracking, good tensile, fatigue, creep, and rupture strength.

Table 1: Chemical composition of studied materials (wt.%)

[%]	FB2	17-4-PH	625M	IN718
C	0.13	0.07	0.03	0.08
Mn	0.35	1.0	0.5	0.35
P	-	0.04	0.015	0.015
Cr	9.3	15-17.5	20-23	17-21
Mo	1.50	-	8-10	2.8-3.3
V	0.20	-	-	-
Al	-	-	0.4	0.20-0.80
S	-	0.03	0.015	0.015
Si	-	1	0.15	0.35
Nb	0.05	0.15-0.45	3.15-4.15(Nb+Ta)	4.75-5.5
N	0.020	-	0.2	-
Ni	0.1	3-5	58	50-55
B	0.01	-	-	0.0006
Ti	-	-	0.4	0.65-1.15
Fe	Bal.	Bal.	5	Bal.
Co	1.3	3-5	1	1
Cu	-	-	-	0.3
Ta	-	-	-	0.058

The test samples with the dimensions of 40 mm × 10 mm × 2 mm were made of tubes delivered by RINA

(project partner of the sCO2 FLEX project). Prior to the test, the samples were ground up to 600 grit SiC paper, which is more representative of industrial surfaces, rather than fine polishing, then rinsed with deionized water, alcohol, and dried. The composition of the sCO2 atmosphere was 99.995% in the corrosion experiment.

After the corrosion tests, the weight gains of the investigated materials were measured before and after the test using a Radwag AS 82/220.R2 Plus Analytical Balance. All the samples were weighed on an electronic balance with an accuracy of 0.00001 g. Mirco-analysis of the surface corrosion products were characterized by Light Optical Microscope (LOM) and by Scanning Electron Microscopy (SEM) with Energy Dispersive Spectroscopy (EDS). An Olympus BX51P was used for characterization of the surface observation. A LYRA3 Tescan SEM integrated with EDS system was used for characterizing the morphology and compositions of the surface oxide corrosion product layer in both plan and cross-sectional views of the samples.

RESULTS AND DISCUSSION

Weight gain

Tab. 2 showed the weight gain of experimental materials in sCO2 after exposition. The table shows the average value of the weight gain, that came from 3 parallel specimens. The measurement error is 0.015 mg. After 1000 h exposure, Tab. 2 showed that martensitic steel FB2 exhibited the largest weight gain, while others showed a much lower but similar weight gain. Relatively thin and continuous Cr_2O_3 layer would be formed on alloys containing at least 14 % Cr in high-temperature sCO2 as reported in work Subramanian [20]. In718 with a higher Cr and Ni concentration showed the best corrosion resistance in a high-temperature sCO2 environment.

Table 2: Weight gain of the investigated materials in sCO2

Sample	Mass change [%]
FB2	1.17013
17-4-PH	0.00517
625M	0.00675
In718	0.00049

Characterization of the corrosion products

Fig. 5, 6, 7, 8 showed the surface morphology of the investigated materials in sCO2 after exposure. Numerous lumpy structure and pronounced hillock oxides were observed on FB2, as shown in Fig. 5 b,c. As can we seen the Fig. 5a before exposure, the oxidation process is very significant in comparison with Fig. 5 b,c,d.

The continuous, thin oxide was observed on 17-4-PH in Fig. 6 b,c,d. The oxide formed on the surface doesn´t copy the grooves after mechanical surface treatment. Structure of this oxide is very similar like FB2, but thinner.

Many irregular, and discontinuous oxides were found on 625M and In718 in Fig. 7, 8 b,c,d. Different shades on the surface indicate different thicknesses and probably is possible the change in composition. Notably, numerous micrometer-sized nodular oxides were detected on In718 in Fig. 8 d.

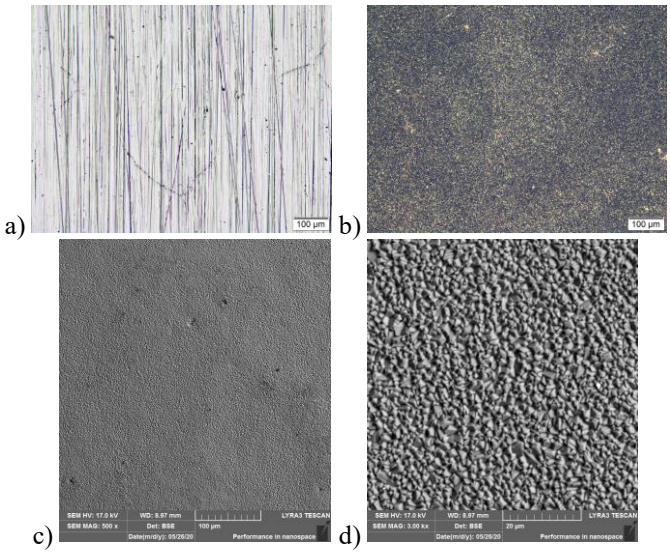

Figure 5: Surface morphologies of the FB2 before (a) and after sCO2 exposure (b,c,d)

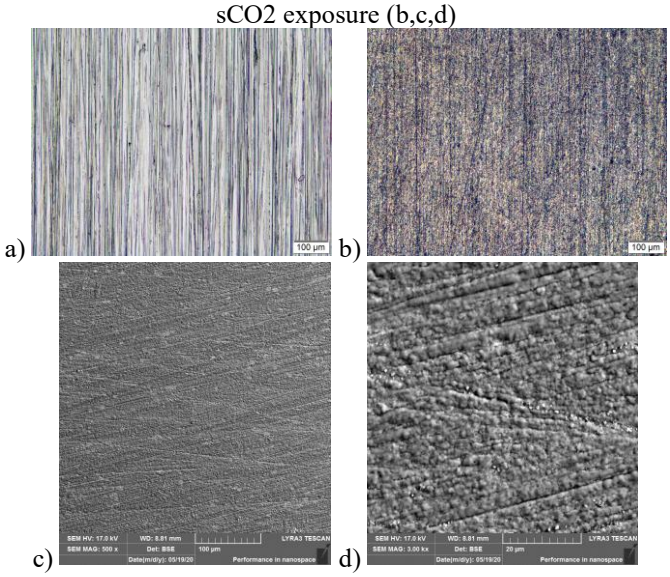

Figure 6: Surface morphologies of the 17-4-PH before (a) and after sCO2 exposure (b,c,d)

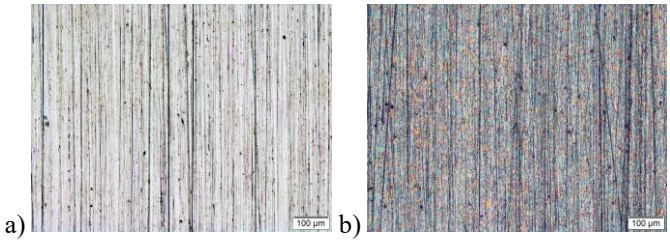

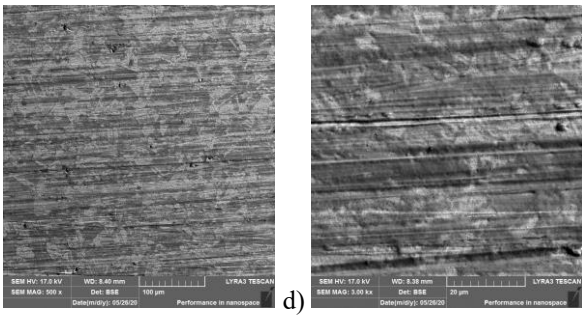

c) d)

Figure 7: Surface morphologies of the 625M before (a) and after sCO2 exposure (b,c,d)

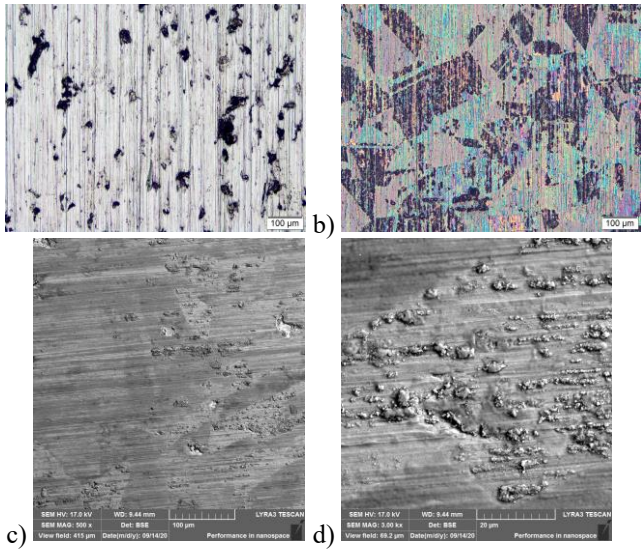

a) b) c) d)

Figure 8: Surface morphologies of the In718 before (a) and after sCO2 exposure (b,c,d)

Fig. 9-12 showed the cross-sectional morphologies of the investigated materials in exposure of sCO2.

Surface observation showed the formation of oxide layer on the Fe-base. The oxide layer was thick and homogeneous all over the surface. Cross section of this material confirmed the thick homogeneous oxide layer without cracks and defects as can we seen on the Fig. 9. The oxide layer consists from the inner and outer layer, outer is on the Fe-base and inner is formed from the Fe-Cr-O spinel. Under the main layer is internal oxidation zone which is formed from mixed oxide on the Fe-Cr-O base. The thickness of these layers is around 22 µm for outer and around 18 µm for inner. The outer layer was formed by the diffusion of metal elements to the outside and the inner layer was formed by that of oxygen to the inside.

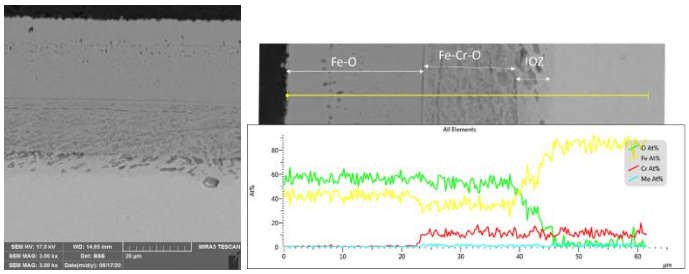

Figure 9: SEM cross section of the FB2 and EDX linescan of the oxide layer

On the martensitic steel 17-4-PH surface was formed the oxide layer. Optical surface analyses showed the different oxide thickness which means variability of colors. This claim confirms cross section observation on the Fig. 10. Cross-section observation showed the formation of either a single Cr-O layer and also localized duplex spinel oxide. Duplex spinel oxide is formed from outer Fe-O layer and inner Fe-Cr-O spinel. Fe-Cr-O spinel is formed inside to the steel.

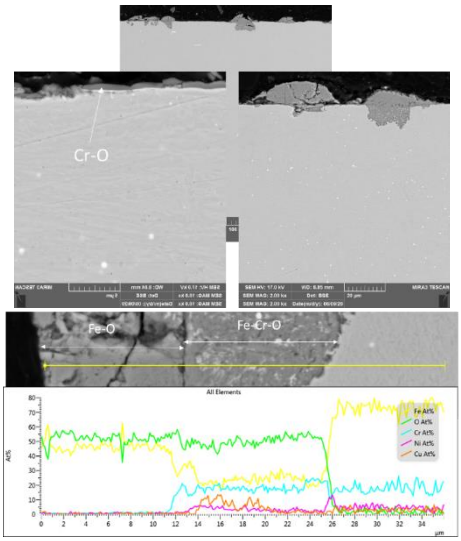

Figure 10: SEM cross section of the 17-4-PH and EDX linescan of the oxide layer

The surface of alloy 625M after exposure in sCO2 is shown in Fig. 7, and the surface oxide was clearly observed and the different surface colours from LOM and SEM suggest the different thickness of the oxide on the surface, which is confirmed by the analysis in cross-section. Fig. 11 shows the EDS linescan of the oxide layer after exposure. According to the cross-sectional morphologies, the corrosion products on the 625M were composed of an outer layer of Cr-Ni-O, and an inner layer of Ni-Cr-O with depleted Cr part. The oxide layer was no homogeneous around all observed surface in cross-section observation.

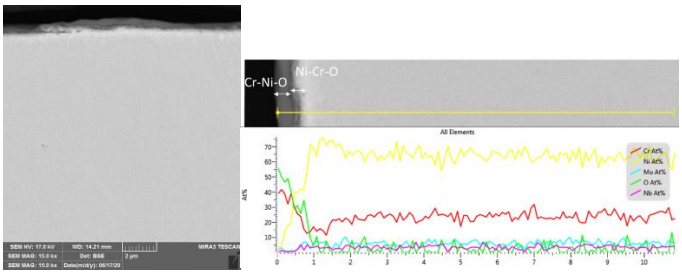

Figure 11: SEM cross section of the 625M and EDX linescan of the oxide layer

Fig. 8 showed the surface observation by LOM and SEM, these analyses showed the uneven oxidation. This claim confirms the cross-section observation as can we seen in Fig. 12. The Ni-base alloy In718 have a sufficient amount of Fe to develop an outer layer on the Fe-O, as shown in Fig. 12 linescan. Under the outer layer was observed the depleted part of Ni and Cr. The cross-section also suggests the creation of the cracks or defects, probably.

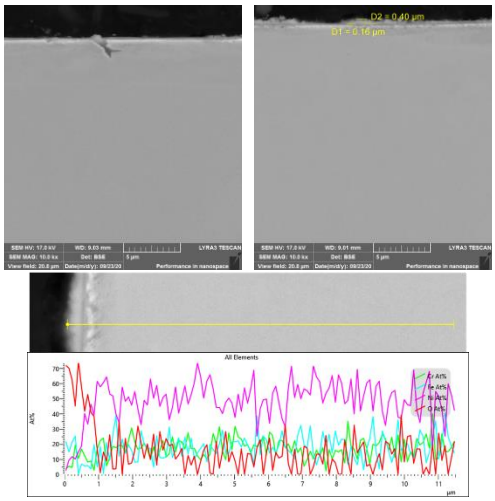

Figure 12: SEM cross section of the In718 and EDX linescan of the oxide layer

CONCLUSIONS

I. The weight gain of the corrosion products corresponded with Cr content in base material, where is obvious that the less content of chromium and high content of iron they tend to create of oxide layer. These claims are also supported by the works of Gui, Furukawa, Tan [4, 11, 16, 17].

II. FB2 has greater weight gain compared to other steels selected for sCO2 power cycle components. This sample has thick and compact duplex layer on the surface, which could with time increase the thickness of outer layer with subsequent spalling. This can be reason of circuit pollution with the corrosion layers.

III. 17-4-PH showed the very different behaviour in comparison to the other studied materials, because as the only one to form a significant nodules of the oxide like in and out, which can cause the corrosion attack over the significant oxidation layer inside in material.

IV. Chromia-forming alloys 625M and In718 showed better corrosion resistance than the FB2 and 17-4-PH due to the formation of the Fe-oxide or Cr-oxide rich scales on its surface. This result was mainly attributed to the higher Cr content in alloys 625M and In718. It was demonstrated that the corrosion performance of steels and alloys in supercritical carbon dioxide was mainly decided by the Cr content [4, 11, 16, 17].

V. 625M formed a dense and continuous Cr-O oxide layer with Ni content and exhibited an excellent corrosion resistance in high-temperature sCO2 environment. The sufficient Cr in the interior of the alloy supports the stability of the Cr oxide layer.

ACKNOWLEDGEMENTS

The presented work was financially supported by the H2020 sCO2-FLEX project. This project has received funding from the European Union's Horizon 2020 research and innovation programme under grant agreement N° 764690.

Some of presented results were obtained with support of Technology Agency of Czech Republic, project "Purification and purity control of CO2 gas in power cycles" No. TK02030023.

REFERENCES

[1] F. Crespi, G. Gavagnin, D. Sánchez, G.S. Martínez. (2017). Supercritical carbon dioxide cycles for power generation: a review. Appl. Energy, 195, 152-183.
[2] M.-J. Li, H.-H. Zhu, J.-Q. Guo, K. Wang, W.-Q. Tao. (2017). The development technology and applications of supercritical CO2 power cycle in nuclear energy, solar energy and other energy industries. Appl. Therm. Eng., 126, 255-275.
[3] V. Dostál. (2005). A Supercritical Carbon Dioxide Cycle for Next Generation Nuclear Reactors, 154.
[4] Y. Gui, Z. Liang, H. Shao, Q. Zhao. (2020). Corrosion behavior and lifetime prediction of VM12, Sanicro 25 and Inconel 617 in supercritical carbon dioxide at 600 °C. Corrosion Science, 175, 108870.
[5] Y. Le Moullec. (2013). Conceptual study of a high efficiency coal-fired power plant with CO2 capture using a supercritical CO2 Brayton cycle. Energy, 49, 32-46.
[6] B.A. Pint, J.R. Keiser. (2016). Supercritical CO2 Compatibility of Structural Alloys at 400-750 C. Oak Ridge National Lab. (ORNL), Oak Ridge, TN (United States).
[7] A. Meyer, B. Jacob, M. M. Anderson, K. Sridharan. Effect of supercritical CO2 on the performance of 740H fusion welds. Materials Science and Engineering: A, 742, 2019, 414-422.
[8] B. Pint, J. Keiser. (2015). Initial Assessment of Ni-Base Alloy Performance in 0.1 MPa and Supercritical CO2.
[9] G. Angelino. (1968). Carbon dioxide condensation cycles for power production. J Eng Power, 90, 287-295.
[10] E. Feher. (1968). The supercritical thermodynamic power cycle. Energy Convers Manage, 8, 85-90.

[11] T. Furukawa, Y. Inagaki, M. Aritomi. (2011). Compatibility of FBR structural materials with supercritical carbon dioxide. Prog. Nucl. Energy, 53, 1050-1055.
[12] G.R. Holcomb, C. Carney, Ö.N. Doğan. (2016). Oxidation of alloys for energy applications in supercritical CO2 and H2O. Corros. Sci., 109, 22-35.
[13] D.J. Young, T.D. Nguyen, P. Felfer, J. Zhang, J.M. Cairney. (2014). Penetration of protective chromia scales by carbon. Scr. Mater., 77, 29-32.
[14] F. Rouillard. (2012). Corrosion of 9Cr steel in CO at intermediate temperature III: modelling and simulation of void-induced duplex oxide growth. Oxid. Met., 77, 71-83.
[15] Y. Gui, Z. Liang, Q. Zhao. (2019). Corrosion and carburization behavior of heat-resistant steels in a high-temperature supercritical carbon dioxide environment. Oxid. Met., 92, 123-136.
[16] L. Tan, M. Anderson, D. Taylor, T.R. Allen. (2011). Corrosion of austenitic and ferritic-martensitic steels exposed to supercritical carbon dioxide. Corros. Sci., 53, 3273-3280.
[17] H.J. Grabke. (1972). Oxygen transfer and carbon gasification in the reaction of different carbons with CO2. Carbon, 10, 587-599.
[18] H.J. Grabke, I. Wolf. (1987). Carburazation and oxidation. Mat. Sci. Eng., 87, 23-33.
[19] T. Gheno, D. Monceau, J. Zhang, D.J. Young. (2011). Carburisation of ferritic Fe–Cr alloys by low carbon activity gases. Corros. Sci., 53, 2767-2777.
[20] G.O. Subramanian, H.J. Lee, S.H. Kim, C. Jang. (2018). Corrosion and carburization behaviour of Ni-xCr binary alloys in a high-temperature supercritical-carbon dioxide environment. Oxid. Met., 89, 683-697.

DOI: 10.17185/duepublico/73951
URN: urn:nbn:de:hbz:464-20210330-095215-5